



## Particle dispersion in homogeneous turbulence using the one-dimensional turbulence model

Guangyuan Sun, David O. Lignell, John C. Hewson, and Craig R. Gin

Citation: [Physics of Fluids \(1994-present\)](#) **26**, 103301 (2014); doi: 10.1063/1.4896555

View online: <http://dx.doi.org/10.1063/1.4896555>

View Table of Contents: <http://scitation.aip.org/content/aip/journal/pof2/26/10?ver=pdfcov>

Published by the [AIP Publishing](#)

---

### Articles you may be interested in

[Dispersion and temperature statistics of inertial particles in isotropic turbulence](#)

Phys. Fluids **22**, 063301 (2010); 10.1063/1.3392772

[Consistent modeling of interphase turbulent kinetic energy transfer in particle-laden turbulent flows](#)

Phys. Fluids **19**, 085101 (2007); 10.1063/1.2756579

[One-dimensional turbulence: Variable-density formulation and application to mixing layers](#)

Phys. Fluids **17**, 025107 (2005); 10.1063/1.1847413

[Direct numerical simulation of particle dispersion in homogeneous turbulent shear flows](#)

Phys. Fluids **13**, 3346 (2001); 10.1063/1.1405443

[A Lagrangian model for turbulent dispersion with turbulent-like flow structure: Comparison with direct numerical simulation for two-particle statistics](#)

Phys. Fluids **11**, 1572 (1999); 10.1063/1.870019

---

The logo for AIP Chaos, featuring the letters 'AIP' in a large, white, sans-serif font, followed by a vertical yellow bar and the word 'Chaos' in a smaller, white, sans-serif font. The background is a dark red gradient with abstract, light red, geometric patterns.

AIP | Chaos

**CALL FOR APPLICANTS**  
Seeking new Editor-in-Chief

## Particle dispersion in homogeneous turbulence using the one-dimensional turbulence model

Guangyuan Sun,<sup>1,a)</sup> David O. Lignell,<sup>1,b)</sup> John C. Hewson,<sup>2,c)</sup>  
and Craig R. Gin<sup>3,d)</sup>

<sup>1</sup>*Chemical Engineering Department, Brigham Young University, Provo, Utah 84602, USA*

<sup>2</sup>*Fire Science and Technology Department, Sandia National Laboratories, Albuquerque, New Mexico 87123, USA*

<sup>3</sup>*Department of Mathematics, Texas A&M University, College Station, Texas 77843, USA*

(Received 19 April 2014; accepted 11 September 2014; published online 9 October 2014)

Lagrangian particle dispersion is studied using the one-dimensional turbulence (ODT) model in homogeneous decaying turbulence configurations. The ODT model has been widely and successfully applied to a number of reacting and nonreacting flow configurations, but only limited application has been made to multiphase flows. Here, we present a version of the particle implementation and interaction with the stochastic and instantaneous ODT eddy events. The model is characterized by comparison to experimental data of particle dispersion for a range of intrinsic particle time scales and body forces. Particle dispersion, velocity, and integral time scale results are presented. The particle implementation introduces a single model parameter  $\beta_p$ , and sensitivity to this parameter and behavior of the model are discussed. Good agreement is found with experimental data and the ODT model is able to capture the particle inertial and trajectory crossing effects. These results serve as a validation case of the multiphase implementations of ODT for extensions to other flow configurations.

© 2014 AIP Publishing LLC. [<http://dx.doi.org/10.1063/1.4896555>]

### I. INTRODUCTION

The motion and dispersion of particles in turbulent flow has important applications in many areas of engineering.<sup>1,2</sup> As an example, turbulent reacting flows like those found in combustion often interact with particles in the form of droplets that might be a source of fuel, a source of fire suppressant, or a hazardous material to be incinerated. Particles are dispersed throughout the flow field by the action of turbulence, and the extent of that dispersion is an important factor in designing effective systems. It is particularly important to determine the differences in dispersion associated with differences in relative inertia between particles and the fluid.

One of the earliest predictive models for particle dispersion was developed by Einstein to describe Brownian motion through a distribution of displacements at a rate given by thermal energy.<sup>3,4</sup> Taylor related turbulent fluid particle dispersion to the velocity fluctuations and their degree of correlation over time,<sup>5</sup> while Batchelor extended this to multidimensional dispersion.<sup>6</sup> These concepts were directly extensible to particle dispersion, where rather than the fluid velocities and their Lagrangian autocorrelation time, the particle velocities and particle autocorrelation time are appropriate

$$\langle x^2 \rangle = 2 \int_0^t \int_0^{t'} v(0)v(\tau) d\tau dt', \quad (1)$$

where  $v$  represents the particle velocities.

a)Electronic mail: [gysungrad@gmail.com](mailto:gysungrad@gmail.com)

b)Electronic mail: [davidlignell@byu.edu](mailto:davidlignell@byu.edu)

c)Electronic mail: [jchewso@sandia.gov](mailto:jchewso@sandia.gov)

d)Electronic mail: [cgin@math.tamu.edu](mailto:cgin@math.tamu.edu)

The particle velocities evolve according to the forcing introduced by the fluid drag, body forces, and other forces as appropriate (such as the Saffman lift force in velocity gradients<sup>7,8</sup>). A challenge arises then because the fluid velocity at the particle location is required, and this fluid velocity is often solved only in an averaged or filtered sense due to the cost of direct numerical simulations (DNS). There are a number of approaches to modeling the instantaneous fluid velocities. The general approach involves the determination of statistical moments for the fluid velocity, the assumption of a distribution of fluid velocities from those moments that act over a given time scale (referred to as an eddy-interaction time), and the deterministic evolution of the particle forced by the given fluid velocity for a sequence of eddy-interaction times.<sup>1,9,10</sup> These approaches have found significant success, and their incorporation within large-eddy simulations (LES), where large scale anisotropy is resolved, leads to further improvement.

Here, we describe an alternate approach. Rather than carry out a separate determination of the fluid moments and a sampling of expected fluid velocities, we integrate the particle evolution with a reduced dimension stochastic approach to evolve the flow field. This approach is referred to as the one-dimensional turbulence (ODT) model.<sup>11-14</sup> Within the context of ODT fluid velocities and any associated scalars are fully resolved in a single dimension. Molecular processes like viscous dissipation evolve through a deterministic process along that single dimension, while the nonlinear turbulent cascade is modeled through a remapping procedure that reproduces key aspects of turbulent flows.<sup>15</sup> By carrying out a fully resolved temporal flow evolution in a single spatial dimension, the one-dimensional spectrum of velocity and scalar fluctuations is available and associated with a given physical location. A particle associated with that same physical location would then accelerate according to the velocity at that point and the appropriate drag law.

ODT has previously been used to study a wide range of fluid mixing applications, in reacting and nonreacting flows, that demonstrate its ability to predict fluid particle dispersion in analogy to scalar mixing.<sup>15-19</sup> However, very limited work has been performed with ODT in multiphase flow: Schmidt *et al.* studied wall deposition of inertial particles in channel flow using ODT.<sup>20</sup> In order to apply the ODT model to the study of a broader range of multi-phase flows, a validation and characterization of the model behavior is required. The goal of the present work is to evaluate the performance of ODT with particles in relatively simple homogeneous isotropic turbulence and to fully describe the sensitivity of predictions to a parameter that appears in the model. While the present work focuses on the evolution of the particles in conjunction with the fluid velocity field, additional value will come through the joint evolution of the more complete fluid state, such as including a temperature field and its correlation with the velocity evolution. For example, an important area of research is the transport and interaction of inertial particles with a flame. Characterization of such transport requires detailed information of particle-flame-flow statistics. DNS provides such information, but at relatively high computational cost and at a limited range of scales. The successful application of ODT to multiphase flows may provide an additional tool for investigating such flows, especially if combined with DNS and experimental data.

The present work focuses on the process of particle dispersion within the ODT context. In this, it draws on the previous work of Schmidt and co-workers where the original Lagrangian particle tracking models within the ODT context were developed.<sup>20,21</sup> Applications here focus on characteristics of ODT particle dispersion of finite Stokes number particles in homogeneous turbulence as experimentally manifest in grid-generated turbulence.<sup>22,23</sup>

There are two phenomena of interest related to finite-Stokes number particles. First, inertial particles will have some slip relative to the fluid since they respond more gradually to accelerations. This leads to reduced particle fluctuations relative to the fluid.<sup>22,24</sup> Second, particles acted on by body forces will have a finite mean velocity that tends to reduce the autocorrelation time as observed by particles in what Yudine<sup>25</sup> referred to as the “effect of crossing trajectories.” This arises because the particles continuously change their fluid environment and are not acted upon for as long as a given eddy lifetime. We will show here that the ODT particle dispersion model captures both of these phenomena through comparison with measurements in Sec. III and through analysis of the model itself in Sec. IV. First, we review the ODT model and describe two approaches to coupling particle evolution with the ODT model in Sec. II. We then present results of the particle dispersion in

Sec. III, followed by a discussion focusing on the sensitivity of various statistics to the ODT particle parameter  $\beta_p$  in Sec. IV.

## II. MODEL FORMULATION

This section summarizes the ODT model and its implementation, along with the Lagrangian particle models applied and developed. In the following discussion,  $y$  is the line direction,  $x$  is the streamwise flow direction (when relevant, as in grid turbulence), and  $z$  is a spanwise direction. The ODT line is generally aligned with the direction of mean shear (cross-stream, as in jets), although in the grid turbulence studied here it is along one of the directions transverse to the flow.

### A. ODT model description

The ODT model used in this study has been described in detail in Ref. 14. A brief summary and description of the model is provided in this section and parallels the discussion in Ref. 19. ODT is a stochastic model for turbulent flows that solves the unsteady, one-dimensional transport equations (diffusion equations) for mass, momentum, and optionally other scalars, such as energy and chemical species. Because the model is one-dimensional, turbulent advection cannot be computed directly. Instead, effects of turbulent advection are modeled by a stochastic mapping processes called eddy events that are implemented as so-called triplet maps, which rearrange fluid in the domain in a manner consistent with turbulent scaling laws. These eddy events are performed concurrently with the solution of the diffusion equations.

Eddy events are parameterized by the eddy location  $y_0$ , eddy size  $l$ , and corresponding eddy timescale  $\tau_e$  that depends on  $y_0$  and  $l$ . The size, location, and frequency of eddies occur stochastically on the domain as described below. Each eddy event is implemented as a triplet map that consists of replacing each scalar in the eddy region with three copies of the scalar, each compressed spatially by a factor of three and lined up along the eddy region, with the central copy spatially inverted. The triplet map is consistent with the behavior of a canonical turbulent eddy in that it is continuous, conservative of all quantities (measure preserving), increases scalar gradients, and decreases length scales locally (by the factor-of-three compression). This compression is facilitated in the current implementation by the use of an automatically adapted computational grid, with assumed piecewise-constant scalar profiles in each grid control volume. An adaptive grid is convenient, but not necessary, as several discrete implementations have been used (including the original implementation of the model<sup>11</sup>). The adaptive formulation avoids the need for a discrete transport correction,<sup>26</sup> and eddy sizes are not limited to multiples of three times the grid spacing. In the present implementation, grid cells are split where the edges of the eddy intersect the cell.

The specification of eddies is dependent on the spatially evolving momentum fields. Eddies are more likely in regions of high shear, and shear is locally increased by triplet maps, resulting in an eddy cascade. The diffusive advancement of the velocity fields smooths the flow with viscous dissipation concentrated at the smallest scales.

Eddies occur stochastically on the domain as follows. For any given eddy ( $y_0, l$ ), there is an eddy timescale  $\tau_e(y_0, l)$  defined by the scaling  $E_{\text{kin}} \approx \frac{1}{2}\rho l^3/\tau_e^2$ , where  $E_{\text{kin}}$  is a measure of the fluid kinetic energy in the eddy region. The eddy timescale  $\tau_e$  is computed as

$$\frac{1}{\tau_e} = C \sqrt{\frac{2}{\rho l^3} (E_{\text{kin}} - Z E_{\text{vp}})}. \quad (2)$$

Here,  $E_{\text{kin}} = \frac{1}{2}\rho l(u_k^2 + v_k^2 + w_k^2)$ , is a measure of the local kinetic energy,<sup>14</sup> and the  $E_{\text{vp}} = \frac{1}{2}\mu^2/\rho l$  term is a viscous penalty to suppress small eddies.  $u_k$  is defined as  $u_k = \frac{1}{l^2} \int_{y_0}^{y_0+l} u(y)K(y)dy$ , where  $K(y)$  is a kernel function equal to the spatial displacements defined by the triplet map;  $v_k$  and  $w_k$  are defined similarly. This measure of the local kinetic energy over the scale  $l$  is analogous to a Fourier coefficient or similar measure of the energy spectrum, and it does not allow a precise determination of the eddy rate. To account for this,  $C$  and  $Z$  are adjustable eddy rate and viscous penalty model parameters, respectively. The parameter  $C$  is important in determining the rate of dissipation, while

the parameter  $Z$  is primarily a numerical expedient to avoid excessive sub-Kolmogorov scale eddy events that are rapidly dissipated.

An eddy rate per position  $y_0$  and per eddy length  $l$  is defined as  $\lambda(y_0, l) = (\tau_e l^2)^{-1}$ . The total rate of all eddies is then  $\Lambda = \int \lambda dy_0 dl$ , and we can define  $P(y_0, l) = \lambda(y_0, l)/\Lambda$  as the joint probability density function (PDF) of eddy sizes and locations. Eddies could then be sampled from  $P(y_0, l)$  at times selected from a Poisson process with mean rate  $\Lambda$ . In practice,  $P(y_0, l)$  is prohibitively expensive to compute since the velocity profiles (hence  $\tau_e$ ) are constantly evolving by diffusive relaxation and stochastic eddy events. This would require continual re-calculation of the two-dimensional PDF. Instead, an analytic estimation of  $P$  is specified, denoted  $\tilde{P}(y_0, l)$ , and is used with a thinning process<sup>27</sup> based on the rejection method.<sup>28</sup> Eddies are sampled from  $\tilde{P}(y_0, l)$ , and accepted with probability

$$P_a = \frac{\Delta t_s}{\tau_e l^2 \tilde{P}(y_0, l)}. \quad (3)$$

Candidate eddy occurrence times are sampled from a Poisson processes with rate  $1/\Delta t_s$ , which is specified to yield an acceptable eddy acceptance probability ( $P_a \ll 1$ ).

The solution evolution procedure is as follows. Beginning with the initial condition, a candidate eddy is sampled from  $\tilde{P}(y_0, l)$ , and the occurrence time is sampled as a Poisson process with mean rate  $1/\Delta t_s$ . The eddy is accepted or rejected with probability  $P_a$  given above. If rejected, the process is repeated, keeping track of cumulative sampled time  $T_{s,c}$ . If accepted, the eddy is implemented, and the diffusion process is solved for a time duration of  $T_{s,c}$ . (Diffusive advancement is also performed to advance the solution in the event that no eddies occur within a small factor of the characteristic grid diffusion timescale.) Further details of the eddy selection procedure, along with the form of  $\tilde{P}(y_0, l)$  are given in Ref. 14.

The time  $\Delta t_s$  is initialized as  $\Delta t_s = 0.1 \bar{P}_a \overline{\Delta y}^2 / \nu n$ , where  $n$  is the number of grid points,  $\nu$  is the kinematic viscosity,  $\overline{\Delta y}$  is the average grid spacing, and  $\bar{P}_a$  is a specified average acceptance probability (here set to 0.02).  $\overline{\Delta y}^2 / \nu$  is a diffusive timescale (approximate lower bound on an eddy timescale) at the grid cell size, and the factor  $1/n$  reflects the proportionality of the total rate to the domain size.  $\Delta t_s$  is dynamically adjusted during the simulation to maintain the specified  $\bar{P}_a$ .

In the vector formulation of ODT (three velocity components evolved), pressure scrambling and return-to-isotropy effects are modeled by adjusting the triplet mapped velocities by adding a term  $c_i K(y)$ , where subscript  $i$  denotes the velocity component, and  $c_i$  is given by<sup>12</sup>

$$c_i = \frac{l^2}{\int_{y_0}^{y_0+l} K(y)^2 dy} \left( -u_{i,k} + \text{sgn}(u_{i,k}) \sqrt{\frac{1}{3} \sum_i u_{i,k}^2} \right). \quad (4)$$

Here, a large eddy suppression mechanism<sup>13,16,18</sup> is incorporated, in which the criteria applied is

$$l \leq \beta_{les} \times L_0(t/t_0)^a, \quad (5)$$

where  $L_0(t/t_0)^a$  is the time-evolving integral scale taken from the experimental measurements<sup>22</sup> where it is found that  $L_0 = 2.8$  cm,  $t_0 = 0.159$  s ( $x/M = 41$ ), and  $a = 0.45$ ;  $\beta_{les}$  is an adjustable parameter that sets limits on improbably large eddy occurrences.

The diffusive advancement portion of the simulation consists of solving three components of the momentum equations (velocity equations). The vector formulation<sup>12</sup> of ODT solves three components of the velocity in order to account for return-to-isotropy effects. They are also important in the particle model discussed below. These velocities are primarily used in specifying the eddy event frequencies, and are solved as scalar momentum equations in the diffusive advancement, but otherwise do not act as advecting velocities (except as detailed in Sec. II B). Advection is modeled with the eddy events.

The solution is evolved on a finite-volume computational grid. A Lagrangian formulation is applied and grid cells are allowed to expand and contract with the flow (which does not occur in the incompressible simulations presented here). The mass balance in this formulation reduces to  $\rho \Delta y = \text{constant}$  for any given grid cell. The momentum equations discretized for a given grid cell

are given by

$$\frac{du_k}{dt} = -\frac{1}{\rho\Delta y}(\sigma_{k,e} - \sigma_{k,w}), \quad (6)$$

where  $u_k$  is one of  $u$ ,  $v$ , or  $w$ , and  $\sigma_k$  is component viscous stress modeled as

$$\sigma_k = -\mu \frac{du_k}{dy}. \quad (7)$$

The subscripts  $e$  and  $w$  denote the east and west cell faces. If a pressure gradient is imposed (in a channel flow, say), the corresponding term is applied to the momentum equations.

The equations are normally solved using the explicit Euler method for efficiency, but the second order Modified Midpoint method<sup>29</sup> is also implemented for comparison. Spatial derivatives are evaluated using second order (on uniform grids) central differences.

Mesh adaption is applied during implementation of eddy events, and before and after diffusive advancement. Grid positions are based on a uniform scalar arc length profile between cells with limitations on the minimum allowed cell size (to avoid unphysically small cells by merging with a neighbor), and a constraint on the relative sizes between two adjacent cells. See Ref. 14 for more details.

## B. Lagrangian particle model

The description and implementation of the Lagrangian particle model is summarized in this section. These models are based on the original work of Schmidt.<sup>20,21</sup> Schmidt outlined several possible Lagrangian particle models in ODT, and implemented one in particular termed *Type-I* that was used to study particle laden channel flow.<sup>20</sup> Here, we summarize our implementation of this model.

For relatively small particles in dilute flows, the following drag law describing the particle motion is used for coordinate direction  $i$ :

$$\frac{dv_{p,i}}{dt} = -\frac{1}{\tau_p}(v_{p,i} - v_{g,i}) + g_i. \quad (8)$$

Here,  $g_i$  is the acceleration associated with any body force,  $\tau_p = \rho_p d_p^2 / 18 \mu f$ , and  $f = 1 + 0.15 Re_p^{0.687}$ , where  $Re_p = \rho_g d_p |\vec{v}_g - \vec{v}_p| / \mu$ . Subscript  $p$  refers to particles and subscript  $g$  refers to the fluid. This paper focuses on fundamental understanding of the behavior of individual particles assuming one-way coupling that ignores the effect of particles on the fluid phase, though two-way coupling during advection and diffusion processes is implemented, and will be described in future work.

In ODT, the turbulent advection process is modeled as a sequence of instantaneous triplet maps as discussed above. The particle evolution according to Eq. (8) suggests a continuous process. This dichotomy leads to at least two alternate approaches to coupling the particle evolution with that of the ODT fluid evolution. The Type-I approach, discussed here, implements particle-eddy interactions (PEIs) as instantaneous displacements, and particle momentum changes according to the instantaneous triplet-map fluid displacements. In this sense, the particle-eddy interactions are in the spirit of Einstein's description of Brownian motion.<sup>4</sup> Another approach, termed Type-C<sup>21</sup> allows eddies to affect particles continuously over the eddy time scale together with the diffusion evolution by mapping the effective eddy velocity over time and space. The Type-C implementation is more analogous to Taylor's description of fluid dispersion.<sup>5</sup> However, the Type-C model does not preserve the tracer-particle limit, which the Type-I model does preserve, discussed below. Due to the importance of Taylor's<sup>5</sup> work, below we derive related quantities for the Type-I approach.

Particles interact with the fluid during the instantaneous eddy events that account for turbulent advection and during the diffusive advancement. During diffusive advancement the particle drag law is integrated (velocity and position) along with the fluid equations. The fluid velocity in Eq. (8) is the local ODT velocity component in the off-line directions, but is zero in the line-direction (for

incompressible flows) since the advection in this direction is treated through the eddy events and continuity implies zero advecting velocity on the one-dimensional ODT line.

The primary advection mechanism through which dispersion is modeled within the context of ODT is through PEIs. An eddy (triplet map) results in fluid displacement and the PEI consists of computing the particle velocity and displacement in response to this fluid displacement during the eddy event. Eddy events occur instantaneously, and in the Type-I model the PEI is also implemented instantaneously. However, to compute the PEI, integration is performed in a so-called PEI time coordinate  $t$ .

In the PEI time coordinate  $t$ , each eddy is conceptualized as a cubical eddy box (though extents in different directions could be varied). In other words, an eddy exists in a defined three-dimensional space for a defined duration. The velocity and the relative motion of the particle and the eddy box are tracked to allow the prediction of the crossing-trajectory effect. The particle is assumed initially to be in the center of the box in the off-line directions ( $x, z$ ), and at its initial location in the line-direction ( $y$ ). The eddy box is stationary in the line-direction as per continuity, but moves in the off-line directions with velocity components equal to the fluid velocity components at the initial location of the particle in the box. An alternative for the off-line box velocities is to use the average of the local ODT velocity components.<sup>21</sup> However, this may result in particles crossing out of the eddy box in the tracer-particle limit (which should not happen) due to the difference in the particle and eddy box velocities.

The particle can interact with an eddy over the minimum of two durations: (1) the duration of the eddy, or (2) the time over which the particle remains within the conceptual eddy box. The eddy duration is related to the eddy rate, Eq. (2), but it is not strictly the inverse of the eddy rate  $\tau_e$ . Rather, the eddy rate is only proportional to a local measure of the velocity fluctuations,  $E_{\text{kin}}$ , over the eddy length  $l$ . To account for the well-known eddy-crossing phenomenon, a measure of this eddy duration is required. For models of the random walk class in the context of  $k$ - $\epsilon$  modeling, this time scale is of the form  $\sqrt{3/2}C_\mu^{3/4}k/\epsilon$  and the eddy length scale is similarly modeled<sup>1,9,10</sup> as  $C_\mu^{3/4}k^{3/2}/\epsilon$ . In those models, a proportionality constant is determined through calibration with experimental data, and a similar approach is required in relating the eddy rate to the eddy duration in ODT. This relation between the eddy rate,  $1/\tau_e$ , and the eddy duration is  $t_{i,\text{max}} = \beta_p \tau_e$ , which is the maximum PEI time. In general,  $t_i = \min(\beta_p \tau_e, t_c)$ , where  $t_c$  is the time at which the particle exits the eddy box. Here,  $\beta_p$  is an adjustable parameter discussed in detail in Sec. IV.

The eddy exit time  $t_c$  is computed by integrating the drag law given in Eq. (8) and solving for the exit time (assuming the particle is not captured by the eddy, in which case  $t_i = \beta_p \tau_e$ ). This is done in all three directions, and the minimum time is taken. The solution to Eq. (8), assuming constant  $f$  in  $\tau_p$ , and using  $dy_{p,i}/dt = v_{p,i}$ , is given by

$$v_{p,i} = v_{g,i} + \tau_p g_i - (\tau_p g_i + v_{g,i} - v_{p,i}^o) e^{-t/\tau_p}, \quad (9)$$

$$y_{p,i} = y_{p,i}^o + v_{g,i} t + \tau_p g_i t - \tau_p (\tau_p g_i + v_{g,i} - v_{p,i}^o) (1 - e^{-t/\tau_p}), \quad (10)$$

where  $v_{p,i}^o$ , and  $y_{p,i}^o$  are the initial particle velocity and location, respectively.

Given the interaction time  $t_i$ , the line-directed particle position  $y_p$  and velocity  $v_p$  are computed by integrating a modified version of the particle drag law for time  $t_i$ . Because the drag law is also integrated during the diffusive advancement in the simulation time coordinate, it is important that the PEI only alters the eddy position and velocity due to the eddy contribution. This is done by taking the difference of the particle velocity computed in Eq. (9) and the particle velocity using the same equation with the gas velocity set equal to zero. The same is done for the particle position. The resulting triplet map-induced changes are

$$\Delta v_p = v_g (1 - e^{-t_i/\tau_p}), \quad (11)$$

$$\Delta y_p = v_g t_i - v_g \tau_p (1 - e^{-t_i/\tau_p}), \quad (12)$$

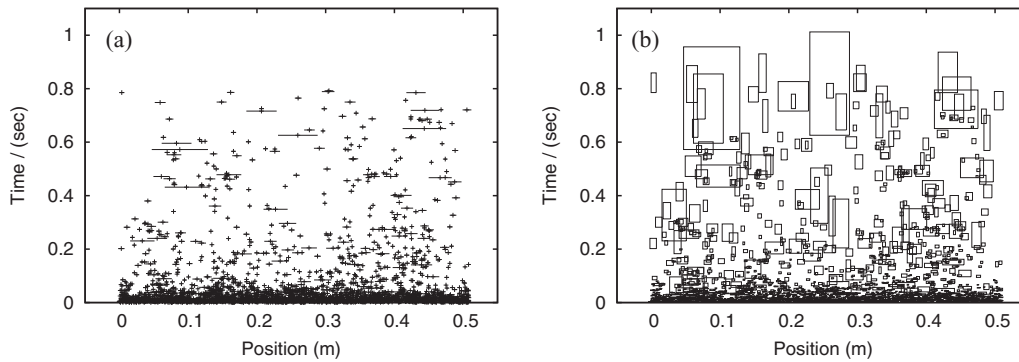


FIG. 1. Maps of eddy sizes, locations, and occurrence times for a typical ODT realization for decaying homogeneous turbulence. Plot (a) shows instantaneous eddy locations; plot (b) shows eddy box extents for the particle eddy interactions (PEI) in the PEI time coordinate  $t$ .

and the post triplet map state is  $v_p = v_p^o + \Delta v_p$ ,  $y_p = y_p^o + \Delta y_p$ . In these equations, the gas velocity is  $v_g = \delta y / \beta_p \tau_e$ , where  $\delta y$  is the local fluid particle displacement defined by the triplet map.

During the PEI, the  $x$  and  $z$  velocity components ( $u$  and  $w$ ) are used only to compute  $t_c$  and hence  $t_i$ , but the particle velocity in those off-line directions is not modified during the PEI process because these particles evolve during diffusive advancement over the full simulation time under the influence of the locally evolving ODT fluid velocity in those directions. As particles are confined to the ODT line, there are no advective displacements of particles in the  $x$  and  $z$  directions. However, since the particles and fluid retain velocity components in these directions, these components may be integrated to study, e.g., streamwise particle dispersion.

Figure 1(a) shows the size, location, and occurrence time of eddies in a typical ODT realization of grid-generated turbulence.<sup>22,23</sup> The instantaneous eddies are denoted by horizontal line segments. The extent of the eddies in the PEI time coordinate  $t$  is depicted in Fig. 1(b), though this does not show the full eddy-box size, and the motion of the eddy boxes as has been described.

The Type-I formulation described has the important and desired effect of satisfying the tracer ( $\tau_p \rightarrow 0$ ) and ballistic ( $\tau_p \rightarrow \infty$ ) limits. In the tracer limit, the final particle position matches the fluid particle position induced by the triplet map since  $\Delta y_p = v_g t_i = \delta y$  for  $t_i = \beta_p \tau_e$  and  $v_g = \delta y / \beta_p \tau_e$ . In the tracer limit, the particle velocity after the eddy is  $v_g = \delta y / \beta_p \tau_e$  (the ODT-aligned eddy velocity component), but relaxes instantaneously to the zero gas velocity during the subsequent diffusive advancement. In the ballistic limit, the particle velocity and position are unchanged by the eddy. Inertial particles show intermediate behavior.

### III. RESULTS

In this section, model predictions are presented, first at the level of properties that can be derived directly from the model and then through comparison with available literature results.

#### A. Grid-generated turbulence

The particle dispersion model is compared to the experimental decaying grid turbulence results of Snyder and Lumley<sup>22</sup> and Wells and Stock.<sup>23</sup> Snyder and Lumley<sup>22</sup> studied the particle motion in a vertical wind tunnel, in which four particle types were used: hollow glass (HG), corn pollen (CP), solid glass (SG), and copper (Cu). The HG particles are similar to fluid particles due to the small particle timescale compared to the Kolmogorov scale. Since the behavior of the solid glass is nearly identical to the copper, results are presented for the HG, CP, and SG particles. Wells and Stock<sup>23</sup> studied glass beads of two sizes in a horizontal wind tunnel, where the particle body force was altered by means of an electric field. Both experimental wind tunnels were operated under

TABLE I. Particle properties of Snyder and Lumley.<sup>22</sup>

	Hollow glass	Corn pollen	Solid glass
Diameter ( $\mu\text{m}$ )	46.5	87	87
Density ( $\text{kg/m}^3$ )	260	1000	2500
$\tau_p f = \rho_p d_p^2 / 18\mu$ (ms)	1.7	23	58

similar conditions with grid spacing  $M = 2.54$  cm and a mean velocity  $U_0 = 6.55$  m/s. The particle properties are listed in Tables I and II.

The ODT simulations are conducted using a 0.508 m (20  $M$ ) domain width. The initial velocity profile is taken as a sine wave (as done by Kerstein<sup>11</sup>):  $u(y, 0) = u_0 \sin(2\pi y/M)$ , where  $u_0 = U\sqrt{2S/(1-S)}$  gives a  $u$  variance in the grid-plane equal to the variance in a uniform profile with  $u = 0$  for a grid-blocked area fraction  $S$ , and  $u = U/(1-S)$  for an open area fraction  $1-S$ . The  $v$  and  $w$  velocity components are initially zero. Simulations were performed using 2048 ODT realizations each with a single particle of a given type initially located in the center of the domain.

Because of the reduced geometrical fidelity inherent in ODT for prediction of actual flows like the decaying wind tunnel turbulence here, some adjustment of model parameters is required, here the root-mean-square (RMS) gas velocity fluctuations and the gas dispersion evolution. To match the measured velocity fluctuations, the ODT parameters  $C = 5.2$  and  $Z = 10$  are determined. Fluid dispersion is sensitive to the acceptance of improbable eddy events, that is, eddies that are accepted even if  $P_a$  in Eq. (3) is small, since these improbable events tend to involve large displacements. To match fluid particle dispersion, we limit the maximum eddy size to a factor of the measured integral length scale as described in Eq. (5) using  $\beta_{les} = 2.4$ . Parameters for Eq. (5),  $t_0 = 0.159$  s and  $L_0 = 0.028$  m, are obtained from measurements by Snyder and Lumley.<sup>22</sup>

The determination and sensitivity of ODT parameters  $C$ ,  $Z$ , and  $\beta_{les}$  has been discussed in the literature.<sup>18,19,30</sup> In general, predictions are sensitive to parameter  $C$  that controls the rate of fluctuation dissipation but insensitive to parameter  $Z$ . The focus of this paper is on particle dispersion, and the sensitivity to the particle parameter  $\beta_p$  is discussed in Sec. IV. The parameter  $\beta_p$  is specified based only on the particle dispersion and independently of the flow parameters  $C$ ,  $Z$ , and  $\beta_{les}$  that are set based on the fluid evolution.

Figure 2 shows the decay of the streamwise RMS velocity compared to the experimental data. Both the measurements and predictions follow a power-law decay with an exponent of  $-1.2$ . The Wells and Stock<sup>23</sup> measurements have a similar  $u'$  decay rate but lower turbulent intensity at a given location; their data agree with Snyder and Lumley<sup>22</sup> when shifted  $15M$  to the right<sup>31</sup> as shown in Fig. 2. The gas decay curve in Fig. 2 can be matched by ODT using no large eddy suppression (with a different  $C$  parameter), but the resulting particle dispersion is incorrect due to the occurrence of unphysically large eddies causing disproportionate particle dispersion.

TABLE II. Particle properties of Wells and Stock.<sup>23</sup>

Diameter ( $\mu\text{m}$ )	Density ( $\text{kg/m}^3$ )	$\tau_p f$ (ms)	Terminal velocity (cm/s)	Particle acceleration ( $\text{m/s}^2$ )
5	2475	0.192	5.86	305.2
			17.06	888.5
			20.91	1089.1
			23.65	1231.8
			0	0
57	2420	24.4	25.8	10.6
			54.5	22.3
			108	44.3

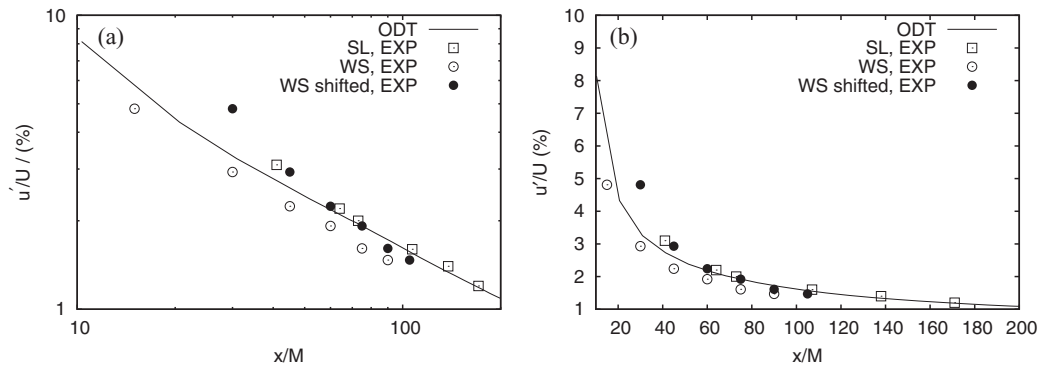


FIG. 2. Normalized RMS streamwise velocity fluctuations: predictions and experiments of Snyder and Lumley<sup>22</sup> (SL), and Wells and Stock<sup>23</sup> (WS) on log (a) and linear (b) scales. The WS shifted data are Wells and Stock measurements shifted 15M to the right.

## B. Particle dispersion

The ODT model mean square dispersion  $\Delta y_p^2$  (where  $\Delta y_p$  is the RMS particle displacement) predictions with  $\beta_p = 0.05$  are shown with experimental measurements from Snyder and Lumley<sup>22</sup> for the three particle types in Fig. 3. The reference position for dispersion of a given particle is consistent with the first experimental camera, which was located at  $x/M = 68$ . The greatest dispersion is obtained by the hollow glass, with dispersion decreasing for the corn pollen and solid glass. The dispersion trend in Fig. 3 is consistent with eddy trajectory crossing being the factor that limits dispersion: particles with larger  $\tau_p$  and larger settling velocities  $v_d$  are less affected by eddies.

To better understand the role of the settling velocity and the crossing trajectory effect, Wells and Stock<sup>23</sup> measured dispersion as a function of  $v_d$  by using charged particles and varying the electric field strength. Figure 4 shows that in ODT particles also disperse less as particle settling velocity,  $v_d = \tau_p g$  (where  $g$  is the resulting electric field acceleration), increases in agreement with the trajectory-crossing theory<sup>24</sup> and measurements.<sup>23</sup> Wells and Stock<sup>23</sup> did not specify the reference position in their published results, and in this study, the particle dispersion is referenced to  $x/M = 15$ . As the results for the 57  $\mu\text{m}$  particles in Fig. 4 show, the crossing-trajectories effect significantly influences dispersion with the different particle terminal settling velocities considered.

Figure 5 compares the evolution of eddy time scale  $\beta_p \tau_e$  with  $\beta_p = 0.05$  to different particle relaxation time scales  $\tau_p$ . The plotted evolution time is relative to the particle dispersion reference location (time zero). The eddy time scale is roughly lognormally distributed, varying over orders of magnitude as expected, and particles in ODT experience the full spectrum of time scales. Other characteristics of lognormally distributed variables are that the mean is larger than the most typical value and that the RMS is comparable to the mean value, both of which are plotted in Fig. 5. The

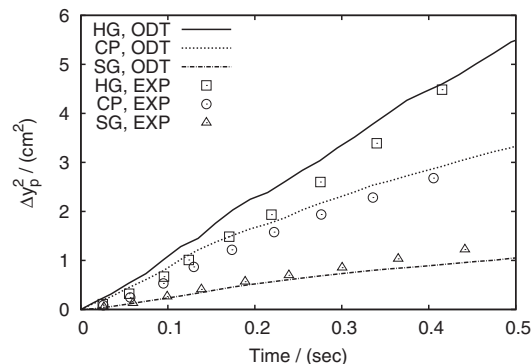


FIG. 3. Comparison of ODT and experimental particle dispersion of Snyder and Lumley.<sup>22</sup>

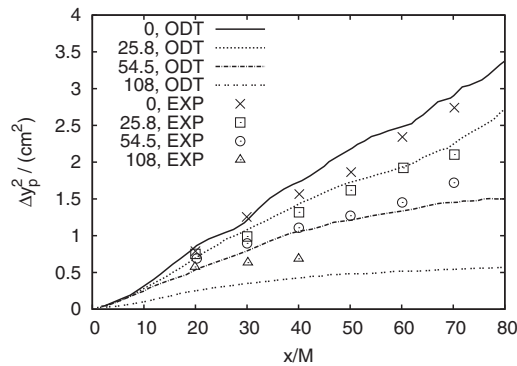


FIG. 4. Comparison of ODT and Wells and Stock<sup>23</sup> particle dispersion for  $57 \mu\text{m}$  particles for four terminal velocities shown in the legend in units of  $\text{cm}^2$ .

Snyder and Lumley<sup>22</sup> particle time scales,  $\tau_p$  are plotted as horizontal lines in Fig. 5. It is seen that a large number of eddies have time scales,  $\beta_p \tau_e$ , smaller than the particle time scales. Initially, most eddies are small and the corn pollen and solid glass particle timescales are greater than the mean eddy timescales. At positive times, the corn pollen and solid glass particles have particle time scales similar to the eddy timescales, though the eddy timescales are generally above the corn pollen timescale, while for the solid glass the mean eddy timescale transitions from above to below the solid glass timescale at around 0.2 s. Conversely, the hollow glass timescale is much smaller than the eddy timescales at positive times.

Particle inertial effect and the crossing trajectory effect are the two most significant features in understanding particle dispersion for configurations studied here. The dispersion coefficient relative to that of a fluid tracer is plotted in Fig. 6 as a function of a dimensionless particle settling velocity analogous to a particle Froude number. The velocity fluctuation used in the normalization is  $u' = 0.1$  m/s. The particle terminal settling velocity is normalized by the fluid RMS velocity fluctuations so that this normalization is equivalent to a normalized particle time constant if the body forces are all equal. The review of Loth<sup>2</sup> shows similar results of finite  $\tau_p$  dispersion coefficients normalized by the tracer dispersion coefficient. For given fixed gravity shown in Fig. 6(a),  $\gamma = v_d/u' = g\tau_p/u'$  is varied by varying  $\tau_p$ . In that figure, small light particles disperse at similar rates to fluid elements, and large heavy particles disperse much less as expected. Figure 6(b) shows results varying the terminal velocity through the externally imposed electric field, for the two particle sizes (separated by the vertical dotted line) measured by Wells and Stock.<sup>23</sup> When the terminal velocity,  $v_d$ , approaches zero, the crossing trajectory effect becomes trivial and particles remain trapped inside an eddy and behave like fluid particles. However, as  $v_d$  increases, particle traversal of the eddy takes over the

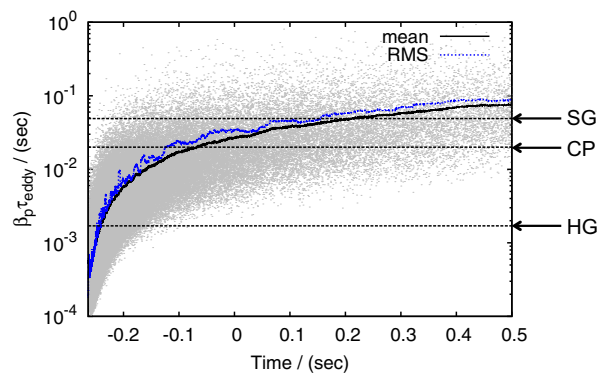


FIG. 5. Scatter plot of eddy time scales with the corresponding mean and RMS along with particle time scales. Time zero is the dispersion reference time. Eddy information is collected from 10 representative realizations.

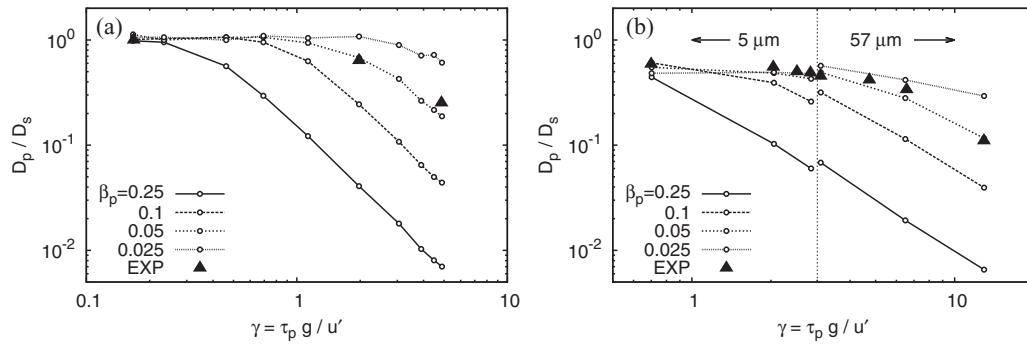


FIG. 6. Normalized particle dispersion versus normalized particle terminal velocity for various  $\beta_p$  (shown in the legends). Plot (a) shows simulation results versus  $\gamma$  where  $\gamma$  is varied by varying  $\tau_p$  (with  $v_d = g \tau_p$ ), and compares to measurements of Snyder and Lumley.<sup>22</sup> Plot (b) shows results versus  $\gamma$  where  $\gamma$  is varied by varying particle acceleration for two particle sizes (5  $\mu\text{m}$  and 57  $\mu\text{m}$  to the left and right, respectively, of the vertical dotted line), compared to measurements of Wells and Stock.<sup>23</sup>

interaction and reduces particle dispersion. ODT predictions in those plots are shown for multiple values of the parameter  $\beta_p$  with the chosen value of  $\beta_p = 0.05$  matching the data well. Further discussion of the effect of  $\beta_p$  is given in Sec. IV. Experimental results are also shown in Fig. 6 for comparison.

### C. Derived statistics

While the Type-I particle-eddy interaction model provides instantaneous displacements as in the Einsteinian approach, it is possible to determine the particle velocity statistics that lead to those displacements. This velocity profile is termed the particle velocity history  $v_{ph}$ , and is computed by modifying the particle velocity computed during the continuous diffusive advancement to account for the advection. For a given PEI, the particle velocity profile for a time  $t_i$  before the eddy occurrence time  $t_{eo}$  is modified so that the particle displacement due to the resulting velocity history is what results from the instantaneous triplet map. That is,

$$v_{ph}(t) = \begin{cases} v_p + v_g(1 - e^{-(t_{eo}-t)/\tau_p}) & \text{if } t_{eo} - t_i \leq t \leq t_{eo}, \\ v_p & \text{otherwise.} \end{cases}$$

This effectively maps the advective velocity in the Type-I PEI time coordinate to the real coordinate so that particle velocity statistics may be computed. Note that  $v_{ph}$  does not affect the actual particle evolution during the simulation but is computed for comparison of ODT results with traditional velocity-fluctuation and correlation-time models.

Given these particle velocity histories, particle velocity statistics are computed for the conditions of the comparisons in the following discussion. Since the velocity fluctuations decay as shown in Fig. 2, statistics are taken 0.2 s after the particle injection reference point ( $x/M = 68$ ). To smooth the velocity statistics, we take advantage of the fact that the inverse particle kinetic energy decay ( $1/v_{ph}^2$ ) is essentially linear with respect to the fluid evolution time, and we compute a linear fit over the simulation time  $0.2 \pm 0.1$  s and interpolate to the statistic of interest at 0.2 s.

The particle velocity fluctuations normalized by the fluid tracer velocity fluctuations are plotted in Fig. 7 as a function of the particle Stokes number,  $St_p = \tau_p/(\beta_p \bar{\tau}_e)$  where  $\beta_p \bar{\tau}_e = 0.053$  is the average eddy time scale at 0.2 s plotted in Fig. 5. The fluid tracer velocity fluctuations are computed similar to the particles by fluid element displacements by triplet maps. The experimental data<sup>22</sup> are also shown normalized by the reported gas turbulence velocities. As expected, particles with larger Stokes numbers experience reduced fluctuations. This is a direct consequence of the dependence of the ratio  $t_i/\tau_p$  appearing in Eq. (11), but two effects contribute to this. Larger  $\tau_p$  or larger Stokes number particles have a reduced response to rapid turbulence fluctuations; that is, the particles act as a low-pass filter because of the ratio of fluid to particle time scales. Also, larger  $\tau_p$  particles have

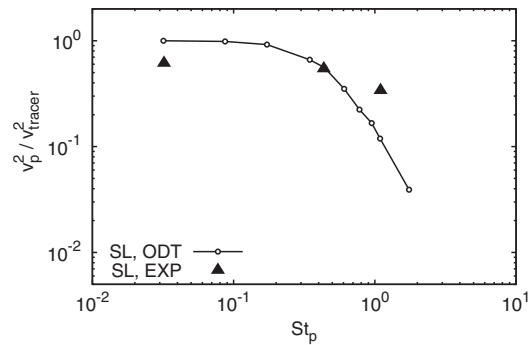


FIG. 7. Particle velocity fluctuation as a function of particle Stokes number.

larger terminal velocities under the influence of body forces leading to a reduction in  $t_i/\tau_p$  through the crossing trajectory effect. These effects will be further discussed in Sec. IV.

The particle velocity histories can also be used to determine the particle Lagrangian integral time scale, or the autocorrelation time. These results have been computed and will be shown as a function of both  $\tau_p$  and  $\beta_p$  in Sec. IV. The product of this particle time scale and the velocity fluctuations in Fig. 7 gives the dispersion coefficient following Taylor's<sup>5</sup> approach. Here, we note that the derived particle velocity history statistics suggest that reduced dispersion at larger  $\tau_p$  (Fig. 6) can be attributed more to variations in the particle velocity fluctuations (Fig. 7) than the integral time scale given the  $\beta_p$  selected here for the ODT model. This will be described further below.

#### IV. DISCUSSION

The implementation of particles into ODT introduces a single parameter,  $\beta_p$ , that relates the turbulence characteristics to the particle-eddy interaction time by scaling the turbulent time scales. This type of parameter is common to other particle-turbulence interaction models.<sup>1,9,10</sup> To allow the model to match the tracer particle limit,  $\beta_p$  plays an additional role in the context of ODT since the triplet-map driven fluid velocities are determined by  $v_g = \delta y / (\beta_p \tau_e)$ . In this section, we discuss the variation in predictions associated with different values of  $\beta_p$ .

In Fig. 6, the predictions of relative particle dispersion coefficients for several values of  $\beta_p$  are given. In the regime where crossing trajectory effects are important (large particle Stokes or Froude numbers), larger  $\beta_p$  results in reduced dispersion. This arises because of the influence that  $\beta_p$  has on the interaction time  $t_i$  together with the eddy velocity  $v_g$ .

The total displacement associated with an eddy is determined by the combination of the displacement during the eddy event given by Eq. (12) and the resulting drift during a deceleration when the particle leaves the eddy with the velocity increment given by Eq. (11):  $\Delta y_p = v_g(1 - \exp(-t_i/\tau_p))$ . For  $v_{p,i}^0 = 0$  and a post-eddy relaxation time much greater than  $\tau_p$  the total displacement per eddy,  $\Delta y_{PEI}$  is  $\Delta y_{PEI} = t_i \delta y / (\beta_p \tau_e)$  (here deterministic displacement due to body forces is not counted). When eddy-crossing is not occurring ( $t_c > \beta_p \tau_e$ ), the interaction time is simply  $t_i = \beta_p \tau_e$  and the displacement per eddy reduces to  $\Delta y_{PEI} = \delta y$ . This is appropriately equivalent to the fluid dispersion and corresponds to the horizontal asymptote in Fig. 6.

Eddy crossing is typically associated with a body-force driven settling velocity. Assuming the particle has reached its terminal velocity, the expected crossing time is  $t_c \approx l/(2g\tau_p)$  where the factor of two assumes the eddy length to be crossed is  $l/2$  on average. With this as the interaction time, when  $t_c < \beta_p \tau_e$  the displacement per eddy is  $\Delta y_{PEI} = l\delta y/(2g\beta_p\tau_e\tau_p)$  leading to the reduced dispersion in this limit seen in Fig. 6.

To better understand the ODT dispersion predictions, it is instructive to identify the scaling present in the model. The particle dispersion coefficient may be written as  $D_p = \Delta y_{PEI}^2 / \Delta t_{PEI}$ , where  $\Delta t_{PEI}$  is the time between eddy interactions. Taking  $\Delta y_{PEI} = l\delta y/(2g\beta_p\tau_e\tau_p)$ , and  $\Delta t_{PEI} = \tau_e$

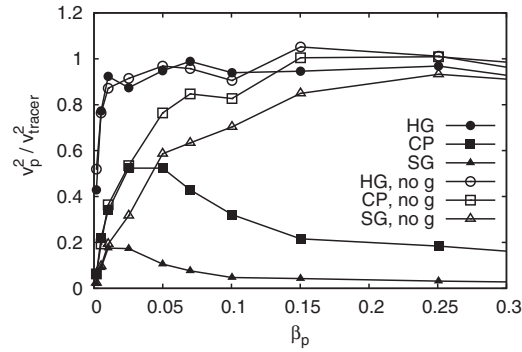


FIG. 8. Prediction of turbulent kinetic energy of particles in the study of Snyder and Lumley<sup>22</sup> with and without gravitational body forces.

gives

$$D_p = \left( \frac{l\delta y}{2g\beta_p\tau_e\tau_p} \right)^2 \frac{1}{\tau_e}, \quad (13)$$

that is,  $D_p \sim 1/\tau_p^2$  in the trajectory-crossing dominated regime. This result is consistent with Fig. 6(a), where the slope of all the simulation curves on the log-log plot is  $-2$  at large  $\tau_p$ .

In the high drift velocity trajectory crossing limit, the rate of eddy interactions is more appropriately  $1/t_i$ . This yields  $D_p \sim 1/\tau_p$ , and gives  $D_p$  essentially the same as that presented by Csanady<sup>24</sup> in the trajectory crossing limit. The  $1/\tau_p^2$  dependence of  $D_p$  in the Type-I model is a consequence of the ODT eddy rate determining the frequency of dispersion events instead of being dominated by the motion of particles from one eddy to another, which would give the rate  $1/t_i = 2g\tau_p/l$ . In cases of high trajectory crossing, a rigorous and physically consistent treatment of the fluid-particle interactions would be to use the spatial formulation of ODT in which the ODT line is advanced in the streamwise direction from one spatial location (perpendicular to the ODT line) to another using boundary layer-type equations.<sup>14</sup> In advancing the ODT line, particles or fluid parcels with higher streamwise velocities have lower implied residence times. Nevertheless, the ODT captures the dispersion well for the range of particles studied here.

Besides scaling the eddy interaction time, the parameter  $\beta_p$  also directly influences the particle velocity by scaling the eddy velocity  $v_g = \delta y/(\beta_p\tau_e)$  in Eqs. (9) through (12). These dual effects complicate the effect of  $\beta_p$  on the particle velocity. Figure 8 shows the particle kinetic energy normalized by that of the tracer particles as a function of  $\beta_p$ . Results are shown with and without gravitational body forces. Values are computed at 0.2 s as in Fig. 7. Particles are known to act as a low-pass filter,<sup>24</sup> following to a lesser degree those motions where  $t_i \ll \tau_p$ . This suggests that for small fluid time scales corresponding to small  $t_i = \beta_p\tau_e$  (or small  $\beta_p$ ) particle fluctuations will be reduced with respect to fluid tracer fluctuations. This behavior is observed in Fig. 8, where the kinetic energy ratio is small for small  $\beta_p$  and rises toward unity with increasing  $\beta_p$  in the no-gravity simulations.

With gravity effects included, similar behavior occurs at small  $\beta_p$ , where the eddy time ( $\beta_p\tau_e$ ) is small so that increasing  $\beta_p$  increases the interaction time, and hence the kinetic energy ratio. Trajectory crossing is minimal for the smallest  $\beta_p$ , but as  $\beta_p$  further increases trajectory crossing occurs, which limits the interaction time to  $t_i = t_c = l/2g\tau_p$  even as the eddy time ( $\beta_p\tau_e$ ) increases. Particles interacting with these longer fluid time scales will see reduced fluctuations because of the reduced interaction time leading to the decay in  $v_p^2/v_{tracer}^2$  for corn pollen and solid glass particles observed in Fig. 8 for large  $\beta_p$ .  $\beta_p$  also affects the point where  $t_c = l/(2g\tau_p) < \beta_p\tau_e$ . The peak in the curves (indicating the transition to trajectory crossing) moves to smaller  $\beta_p$  for larger  $\tau_p$  particles. Note that trajectory crossing is minimal for the HG particles, and the HG curves with and without gravity effects are essentially the same. For  $\beta_p = 0.05$ ,  $v_p^2/v_{tracer}^2$  is significantly reduced for the corn pollen and solid glass as shown in Fig. 7.

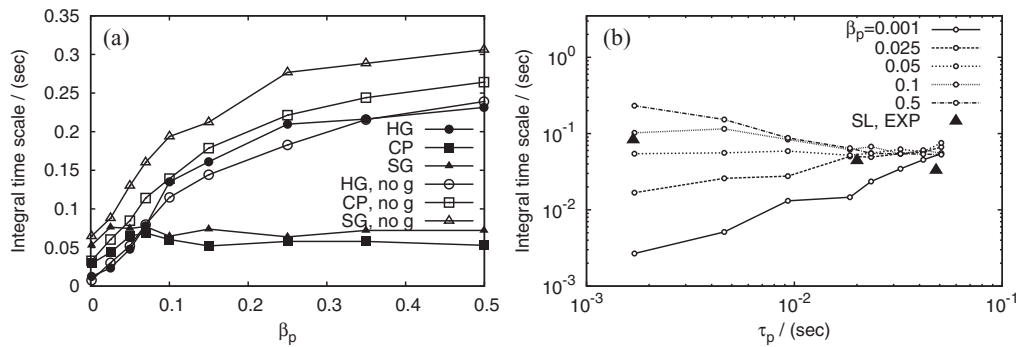


FIG. 9. Prediction of particle autocorrelation integral time scale as a function of  $\beta_p$  with and without body forces (a), and as a function of  $\tau_p$  for hollow glass, corn pollen, and solid glass particles with and without body forces at several  $\beta_p$  (b).

In the approach of Taylor<sup>5</sup> to fluid and particle dispersion, the product of the velocity fluctuations and the autocorrelation time determine the dispersion. In Fig. 9, we plot the Lagrangian particle integral time scale defined from the integral of the particle velocity autocorrelation, computed using  $v_{ph}$ , at the dispersion reference time. Figure 9(a) shows predictions plotted versus  $\beta_p$  for hollow glass, corn pollen, and solid glass particles, both with and without body forces. Figure 9(b) shows similar predictions for the autocorrelation time scale versus  $\tau_p$  for several values of  $\beta_p$ . In the regime where experimental measurements are made, analysis of those measurements suggests that the trajectory crossing effect plays a strong role in reducing the autocorrelation time as the particle time constant increases. Here, we show that this behavior depends on the value selected for  $\beta_p$  in ODT particle dispersion.

The results in Fig. 9 illustrate two competing effects discussed in the next paragraphs: (1) an increase in the autocorrelation integral time scale with increasing  $\tau_p$  in the absence of trajectory crossing; and (2) a decrease in integral time scale with increasing trajectory crossing. The first effect is clear: larger  $\tau_p$  implies a higher particle inertia and a longer response time to imposed fluid fluctuations, which increases the particle autocorrelation and hence the integral time scale. The second effect results from particles that move from one eddy environment with a given local fluid velocity to another, resulting in lower particle velocity correlations and lower integral time scales. Larger  $\tau_p$  particles have higher trajectory crossing due to having a higher terminal settling velocity  $v_d = \tau_p g$ . Hence, higher  $\tau_p$  normally increases the autocorrelation time, but higher  $\tau_p$  results in higher trajectory crossing, which tends to decrease the autocorrelation time.

Consider the autocorrelation time in the absence of body forces (Fig. 9(a) no-g results). In that case, trajectory crossing is minimal, and it is seen that the autocorrelation time increases with  $\tau_p$  due to the increased inertia of the particles. Due to the discrete nature of the eddy velocities, when  $\beta_p$  is small this effect is strong: the relative change in the autocorrelation time is dominated by this inertial effect for small  $\beta_p$ . This is true even when body forces are present. Because this is a consequence of the discrete nature of the ODT displacements and associated profile for  $v_g$ , the authors suggest that the inertial effect described here is stronger than would be experienced in an actual flow. Without body forces, Fig. 9(a), when  $\beta_p$  is large, the discrete changes in the eddy velocity are smaller and  $\beta_p \tau_e / \tau_p$  is large so the integral timescale changes more slowly with  $\beta_p$ .

With body forces present, at small  $\beta_p$  trajectory crossing is still not significant. In this case, Fig. 9(b) with  $\beta_p = 0.001$  shows a clear increase in the autocorrelation time with increasing  $\tau_p$  due to the inertial effect. Conversely, consider the  $\beta_p = 0.5$  case, where trajectory crossing occurs. As  $\tau_p$  increases, the terminal velocity increases, resulting in more trajectory crossing and a shorter interaction time as particles transition from one eddy to another. The decrease in the integral timescale with increasing  $\tau_p$  for this case occurs because the trajectory crossing effect is stronger than the inertia effect. In the limit of high  $\tau_p$  (not shown), this trend reverses: the inertia effect dominates, and the integral scale again increases. In this limit, the integral time scale is not dependent on the value of  $\beta_p$ . At  $\beta_p = 0.05$ , the inertia and trajectory crossing effects approximately balance. The experimental data show a slight decrease, due to trajectory crossing.

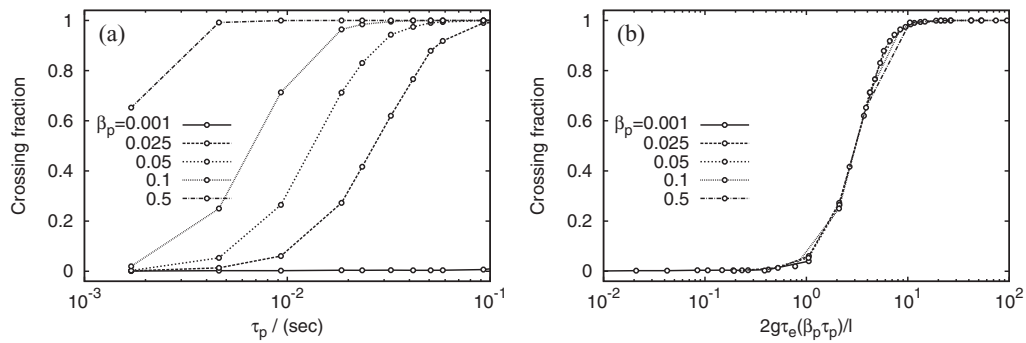


FIG. 10. Fraction of particle eddy interactions that result in particle crossing before the eddy duration  $\beta_p \tau_e$ , for several values of  $\beta_p$ .

As expected, the results are sensitive to  $\beta_p$  because  $\beta_p$  directly scales  $t_{i,max}$ , and hence the trajectory crossing propensity. It is interesting that the ODT model is able to directly probe these effects.

The crossing trajectory dependence on  $\beta_p$  and  $\tau_p$  is highlighted in Fig. 10(a), which shows the fraction of all eddy interactions that result in particles crossing out of the eddy before the eddy is complete (before  $\beta_p \tau_e$ ). These data are computed for times between 0 and 0.5 relative to the dispersion reference time. In smaller time windows, the curve shapes are the same, but slightly shifted as the eddy sizes change relative to the particle timescales (see Fig. 5). At low  $\beta_p$ , almost no eddy crossings occur for any particle  $\tau_p$ . At the highest  $\beta_p$ , particles with  $\tau_p > 0.005$  s nearly always cross the eddies.  $\beta_p = 0.05$  is strongly transitional, and accounts for the relatively small change in the integral time scale for that  $\beta_p$  in Fig. 9(b). That is, as  $\tau_p$  increases, there is an approximate cancellation between the inertial effect tending to increase the integral time scale, and the increasing trajectory crossing tending to decrease the integral time scale.

Figure 10(b) shows the crossing fraction versus the quantity  $R_{pei,ec} = 2g\tau_e(\beta_p\tau_p)/l$ , which is the ratio of the maximum particle-eddy interaction time  $\beta_p\tau_e$  to the eddy crossing time at the terminal velocity,  $t_c = l/(2g\tau_p)$ , given previously. When the crossing fraction is plotted versus this ratio, the predicted crossing fraction versus time ratio collapses onto a single curve. Here,  $\tau_e = 0.95$  s and  $l = 4.1$  mm are taken as the average values in time interval from 0 to 0.5 s. Note that the crossing fraction begins to increase sharply when the time ratio is unity, with nearly all particles crossing eddies when the time ratio exceeds ten. Similar to the crossing fraction, the dispersion coefficients shown in Fig. 6(a) depend on the ratio  $R_{pei,ec}$  and collapse to a single curve when  $D_p/D_s$  plotted versus this ratio. In Fig. 6, the abscissa  $\gamma = \tau_p g/u'$  is equivalent to  $R_{pei,ec}$  if  $u' = l/2\beta_p\tau_e$ .

The ODT particle model presented above is able to capture the key features of particle dispersion for a wide range of particle timescales and body forces. There are several limitations of the model as presented. In a Type-I interaction, the PEIs are necessarily instantaneous. In order to avoid double counting the diffusion processes, a splitting was required in which the PEI is performed using the difference of the velocity and position with and without the eddy velocity, as described above. The instantaneous PEIs complicate the analysis of velocity and position statistics due to the resulting discontinuities in the particle velocity and position fields. The computation of the particle velocity history, described above, allows for the determination of velocity and correlation time statistics. These statistics show the influence of discontinuous eddy velocities, and the present results suggest that these discontinuous velocities lead to reduced autocorrelation times for small  $\tau_p$  particles.

An alternative to the Type-I model is a Type-C model (“C” for continuous). The Type-C model differs from the Type-I model in that the PEI occurs continuously during the continuous diffusive process. While fluid mixing associated with eddies occurs instantaneously, the effect of the eddies on the particles would be implemented over a finite duration during the diffusive advancement. A significant drawback to the Type-C interaction is that it does not obey the tracer-particle limit. The fluid is mapped instantaneously to new locations during an eddy event, but the particles respond to this fluid motion over a finite time during the diffusive advancement. In applications such as

combustion, where particle temperature-history effects are important, the correct tracer-limiting behavior is important.

Another potentially important difference is an apparent time shift. The instantaneous dispersion observed at a time  $t$  in the Type-I interaction is based on the eddy rate at time  $t$ , while a Type-C dispersion, given the eddy rate at time  $t$ , only begins at that time and is not completed until an eddy time scale later. The significance of integral scale fluctuations in dispersion suggests that the Type-C dispersion is delayed by approximately one integral time scale. This is related to matching the tracer limit: in the Type-I model, the motion of particle tracer and fluid element dispersion is the same, while in the Type-C model, the evolution of the particle tracer is delayed relative to the fluid element.

Sensitivity to the  $\beta_p$  parameter was discussed in detail above. It was shown that  $\beta_p$  scales  $t_{i,max}$  and hence the trajectory crossing effect. A single value of  $\beta_p$  was used for a range of  $\tau_p$  and body forces. We advocate setting the  $C$  and  $\beta_{les}$  parameters based on the fluid phase, and  $\beta_p$  based on the particle dispersion. At this point, it is not clear how universal the value for  $\beta_p$  is with respect to other configurations.

The standalone ODT presented here is limited to homogeneous or boundary layer flows. This constrains the particles to the ODT line and may have adverse consequences in cases where the particle velocity is significantly different from the gas velocity in the off-line direction. This is related to the dispersion coefficient dependence on  $\tau_p$ , discussed above. Such differences were not found to be significant here, however, where relatively large particle terminal velocities were present. The ODT model has been extended to three dimensions by coupling lattices of ODT lines that run in three dimensions.<sup>32,33</sup> Such formulations relax the one-dimensional nature of the model and particle-ODT line constraints. In such formulations, three-dimensional structures are captured at an ODT lattice spacing scale, with fine scales resolved in one-dimension. These three-dimensional models may relax the need for the  $\beta_{les}$  parameter, (or rather, the  $\beta_{les}$  parameter may be a fixed factor of the ODT lattice scale). Closure models are also possible for the  $C$  parameter by exploiting consistency between the energy dissipation at the ODT lattice scale and the individual resolved ODT lines.

## V. CONCLUSIONS

A Lagrangian particle model, termed a Type-I model, has been implemented and tested using the one-dimensional turbulence model in decaying homogeneous turbulence configurations. ODT has been widely and successfully applied to a number of nonreacting and reacting flows, but few studies of multi-phase flows with Lagrangian particles have been attempted. The Type-I model has the advantage of matching the tracer and ballistic particle limits, as well as predicting dispersion for intermediately sized inertial particles. A single model parameter  $\beta_p$  is introduced in relating the particle interactions to the stochastic ODT eddy events that model turbulent advection. Results were compared to the experiments of Snyder and Lumley,<sup>22</sup> and Wells and Stock<sup>23</sup> for a range of particle time constants and body forces. Particle dispersion, dispersion coefficients, velocity statistics, and integral time scales were presented. The ODT model generally performs well and is able to capture the particle inertial effects as well as the trajectory crossing effect. Results of derived statistics for particle velocity fluctuations and autocorrelation times suggest that there are some artifacts in the ODT model associated with the discrete nature of the eddy, but these results do not prevent the prediction of dispersion as presented here.

The effects of the model parameter  $\beta_p$  were examined. Larger  $\beta_p$  results in reduced particle dispersion associated with an increased crossing trajectory effect. As expected, the model is found to be sensitive to  $\beta_p$  since  $\beta_p$  directly scales the eddy duration and eddy velocity during particle-eddy interactions. It was shown that the fraction of particle-eddy interactions that result in a particle crossing out of an eddy before the eddy duration  $\beta_p \tau_e$  depends on the ratio  $R_{pei,ec} = 2g\tau_e(\beta_p \tau_p)/l$ . The optimal value of  $\beta_p$  was found to be 0.05 in the present study. Further investigation is needed to determine the sensitivity of  $\beta_p$  to the flow configuration.

The particle model was limited to one-way coupling: that is, particles affected by the fluid, but not vice-versa. The model has been extended to two-way coupling during both eddy events and gas diffusion processes, allowing for higher particle loadings as will be reported separately. The results

presented here represent an important validation case for the ODT model from which extensions to other configurations such as jets and reacting flows may be performed.

## ACKNOWLEDGMENTS

The authors acknowledge helpful discussions with Alan Kerstein. This work was supported by the Defense Threat Reduction Agency under Award No. HDTRA-11-4503I. Sandia National Laboratories is a multi-program laboratory managed and operated by Sandia Corporation, a wholly owned subsidiary of Lockheed Martin Corporation, for the (U.S.) Department of Energy's (DOE) National Nuclear Security Administration under Contract No. DE-AC04-94AL85000.

- <sup>1</sup> J. Shirolkar, C. Coimbra, and M. McQuay, "Fundamental aspects of modeling turbulent particle dispersion in dilute flows," *Prog. Energy Combust. Sci.* **22**, 363–399 (1996).
- <sup>2</sup> E. Loth, "Numerical approaches for motion of dispersed particles, droplets and bubbles," *Prog. Energy Combust. Sci.* **26**, 161–223 (2000).
- <sup>3</sup> A. Einstein, "On the movement of small particles suspended in stationary liquids required by the molecular-kinetic theory of heat," *Ann. Phys.* **17**, 549–560 (1905).
- <sup>4</sup> A. Einstein, "Investigations on the theory of brownian movement," in *Einstein, Collected Papers, Vol. 2, translated by A.D. Cowper*, edited by R. Furth (Dover Publications, Inc., New York, 1926), pp. 170–182, 206–222 (reprinted 1956).
- <sup>5</sup> G. I. Taylor, "Diffusion by continuous movements," *Proc. London Math. Soc.* **20**, 196–211 (1921).
- <sup>6</sup> G. K. Batchelor, "Diffusion in a field of homogeneous turbulence," *Austral. J. Sci. Res., Ser. A* **2**, 437–450 (1949).
- <sup>7</sup> P. Saffman, "The lift on a small sphere in slow shear flow," *J. Fluid Mech.* **22**, 385–400 (1965).
- <sup>8</sup> M. Maxey and J. Riley, "Equation of motion for a small rigid sphere in a nonuniform flow," *Phys. Fluids* **26**, 883–889 (1983).
- <sup>9</sup> A. Gosman and I. Ionnides, "Aspects of computer simulation of liquid fuelled combustors," AIAA Paper No. 81-0323, 1981.
- <sup>10</sup> J. Shuen, L. Chen, and G. Faeth, "Evaluation of a stochastic model of particle dispersion in a turbulent round jet," *AICHE J.* **29**, 167–170 (1983).
- <sup>11</sup> A. R. Kerstein, "One-dimensional turbulence: Model formulation and application to homogeneous turbulence, shear flows, and buoyant stratified flows," *J. Fluid Mech.* **392**, 277–334 (1999).
- <sup>12</sup> A. R. Kerstein, W. T. Ashurst, S. Wunsch, and V. Nilsen, "One-dimensional turbulence: Vector formulation and application to free shear flows," *J. Fluid Mech.* **447**, 85–109 (2001).
- <sup>13</sup> W. T. Ashurst and A. R. Kerstein, "One-dimensional turbulence: Variable density formulation and application to mixing layers," *Phys. Fluids* **17**, 025107 (2005).
- <sup>14</sup> D. O. Lignell, A. R. Kerstein, G. Sun, and E. I. Monson, "Mesh adaption for efficient multiscale implementation of one-dimensional turbulence," *Theor. Comput. Fluid Dyn.* **27**, 273–295 (2013).
- <sup>15</sup> A. R. Kerstein, "Linear-eddy modelling of turbulent transport. Part 6. Microstructure of diffusive scalar mixing fields," *J. Fluid Mech.* **231**, 361–394 (1991).
- <sup>16</sup> T. Echehki, A. R. Kerstein, and T. D. Dreeben, "One-dimensional turbulence simulation of turbulent jet diffusion flames: Model formulation and illustrative applications," *Combust. Flame* **125**, 1083–1105 (2001).
- <sup>17</sup> W. T. Ashurst, A. R. Kerstein, L. M. Pickett, and J. B. Ghandhi, "Passive scalar mixing in a spatially developing shear layer: Comparison of one-dimensional turbulence simulations with experimental results," *Phys. Fluids* **15**, 579–582 (2003).
- <sup>18</sup> J. C. Hewson and A. R. Kerstein, "Stochastic simulation of transport and chemical kinetics in turbulent CO/H<sub>2</sub>/N<sub>2</sub> flames," *Combust. Theory Modell.* **5**, 669–697 (2001).
- <sup>19</sup> D. O. Lignell and D. Rappleye, "One-dimensional-turbulence simulation of flame extinction and reignition in planar ethylene jet flames," *Combust. Flame* **159**, 2930–2943 (2012).
- <sup>20</sup> J. Schmidt, J. Wendt, and A. Kerstein, "Non-equilibrium wall deposition of inertial particles in turbulent flow," *J. Stat. Phys.* **137**, 233–257 (2009).
- <sup>21</sup> J. R. Schmidt, "Stochastic models for the prediction of individual particle trajectories in one dimensional turbulence flows," Ph.D. thesis, The University of Arizona, 2004.
- <sup>22</sup> W. H. Snyder and J. L. Lumley, "Some measurements of particle velocity autocorrelation functions in a turbulent flow," *J. Fluid Mech.* **48**, 41–71 (1971).
- <sup>23</sup> M. R. Wells and D. E. Stock, "The effects of crossing trajectories on the dispersion of particles in a turbulent flow," *J. Fluid Mech.* **136**, 31–62 (1983).
- <sup>24</sup> G. Csanady, "Turbulent diffusion of heavy particles in the atmosphere," *J. Atmos. Sci.* **20**, 201–208 (1963).
- <sup>25</sup> M. Yudine, "Physical consideration on heavy particle diffusion," *Adv. Geophys.* **6**, 185–191 (1959).
- <sup>26</sup> R. J. McDermott, "Toward one-dimensional turbulence subgrid closure for large-eddy simulation," Ph.D. thesis, The University of Utah, 2005.
- <sup>27</sup> P. A. Lewis and G. S. Shedler, "Simulation of nonhomogeneous poisson processes by thinning," *Naval Res. Logistics Quart.* **26**, 403–413 (1979).
- <sup>28</sup> A. Papoulis and S. U. Pillai, *Probability, Random Variables, and Stochastic Processes*, 4th ed. (McGraw-Hill, New York, 2002).
- <sup>29</sup> J. D. Hoffman, *Numerical Methods for Engineers and Scientists* (CRC Press, New York, 2001).
- <sup>30</sup> E. Gonzalez-Juez, A. R. Kerstein, and D. O. Lignell, "Fluxes across double-diffusive interfaces: A one-dimensional-turbulence study," *J. Fluid Mech.* **677**, 218–254 (2011).

- <sup>31</sup>F. Yeh and U. Lei, "On the motion of small particles in a homogeneous isotropic turbulent flow," *Phys. Fluids A* **3**, 2571–2586 (1991).
- <sup>32</sup>E. Gonzalez-Juez, R. Schmidt, and A. Kerstein, "ODTLES simulations of wall-bounded flows," *Phys. Fluids* **23**, 125102 (2011).
- <sup>33</sup>R. C. Schmidt, A. R. Kerstein, and R. McDermott, "ODTLES: A multi-scale model for 3D turbulent flow based on one-dimensional turbulence modeling," *Comput. Methods Appl. Mech. Eng.* **199**, 865–880 (2010).